Current Research (2022) Newfoundland and Labrador Department of Industry, Energy and Technology Geological Survey, Report 22-1, pages 127-146

PETROGRAPHY, GEOCHEMISTRY AND U–Pb GEOCHRONOLOGY OF THE MARTIN LAKE PORPHYRY: 1811 Ma A-TYPE MAGMATISM IN THE SOUTH-CENTRAL NEW QUÉBEC OROGEN

J.P. Butler and M.A. Hamilton[1]
Regional Geology Section
[1]Jack Satterly Geochronology Laboratory, Department of Earth Sciences, University of Toronto, 22 Russell Street, Toronto, ON, Canada M5S 3B1

ABSTRACT

This report presents U–Pb zircon geochronology together with whole-rock lithogeochemical and Sm–Nd isotopic data for the Martin Lake porphyry in the south-central New Québec Orogen (NQO). The unit is a massive feldspar porphyry of unknown stratigraphic affinity situated in the footwall of the Walsh Lake Fault. Field observations and petrographic features suggest that it is probably a subvolcanic intrusion, originally of intermediate composition (perhaps a trachyandesite/latite) that has undergone substantial hydrothermal alteration. Zircon U–Pb geochronology indicates crystallization at 1811.2 ± 3.6 Ma. Trace-element compositions of the porphyry are characterized by strong HFSE enrichment (Zr≈400 ppm, Y≈40 ppm, Nb≈18 ppm) and high Ga (10 000× Ga/Al=2.83–3.72), similar to A-type granites, and combined with Sm–Nd isotopic data ($\varepsilon Nd_{1811\ Ma}$=-4.23; T_{DM}=2399 Ma) point to high-temperature melting of a mixed crustal source with both Archean and relatively juvenile Paleoproterozoic components. The data provide a new upper limit on the timing of deformation in the south-central NQO, and together with previously reported ca. *1813 Ma alkaline magmatism along strike, raise new questions about the lithospheric structure of the NQO at that time.*

INTRODUCTION

The Martin Lake porphyry is a narrow, fault-bounded lens of dark-red feldspar porphyry that crops out in the south-central part of the New Québec Orogen (NQO), just northeast of Martin Lake, Labrador (Auger, 1949; Doherty, 1979; Wardle, 1982). Originally mapped by Auger (1949), the unit has remained somewhat of a mystery owing to its poor exposure and lack of clear field relations, as well as a lack of geochemical and geochronological studies. This report presents petrographic observations from the Martin Lake porphyry coupled with whole-rock lithogeochemical, Sm–Nd isotopic, and U–Pb zircon geochronological data. The studied samples were collected during regional mapping of the Hollinger Lake map area (NTS 23J/16) in the summer of 2017 and 2021, as part of an ongoing effort to constrain the geological history and mineral potential of the Labrador Trough and NQO.

REGIONAL GEOLOGY AND TECTONICS OF THE NEW QUÉBEC OROGEN

The New Québec Orogen is a west-verging Paleoproterozoic orogenic belt that extends approximately 800 km from Ungava Bay southward through northern Québec and western Labrador, where it is truncated by the Mesoproterozoic Grenville Orogen (Figure 1). Detailed reviews of the NQO and its broader tectonic context are provided by Wardle *et al.* (2002) and Corrigan *et al.* (2009, 2018), and only the salient features are described here.

The orogen is generally interpreted as an east-tapering crustal wedge built on underthrust Superior basement resulting from dextral–oblique collision between the Superior Craton and the Core Zone during the terminal phase of the *ca.* 1.92–1.80 Ga Trans-Hudson orogeny (THO; *e.g.*, Dimroth, 1970; Hall *et al.*, 1995; Wardle *et al.*, 2002; Corrigan *et al.*, 2009, 2018, 2021; Konstantinovskaya *et al.*, 2019). It consists of four main lithotectonic domains (*e.g.*, Wardle *et al.*, 2002; Henrique-Pinto *et al.*, 2017): 1) a western autochthonous to parautochthonous domain (Schefferville Zone), comprising low-grade, *ca.* 2.17–1.83 Ga volcano–sedimentary successions of the Kaniapiskau Supergroup (KS; Clark and Wares, 2005; Corrigan *et al.*, 2019); 2) a west-central volcano–sedimentary domain (allochthonous Baby–Howse and Doublet zones), comprising mostly upper levels of the KS (Cycle 2; *see* below) and dominated by *ca.* 1.88 Ga tholeiitic basalts and co-genetic

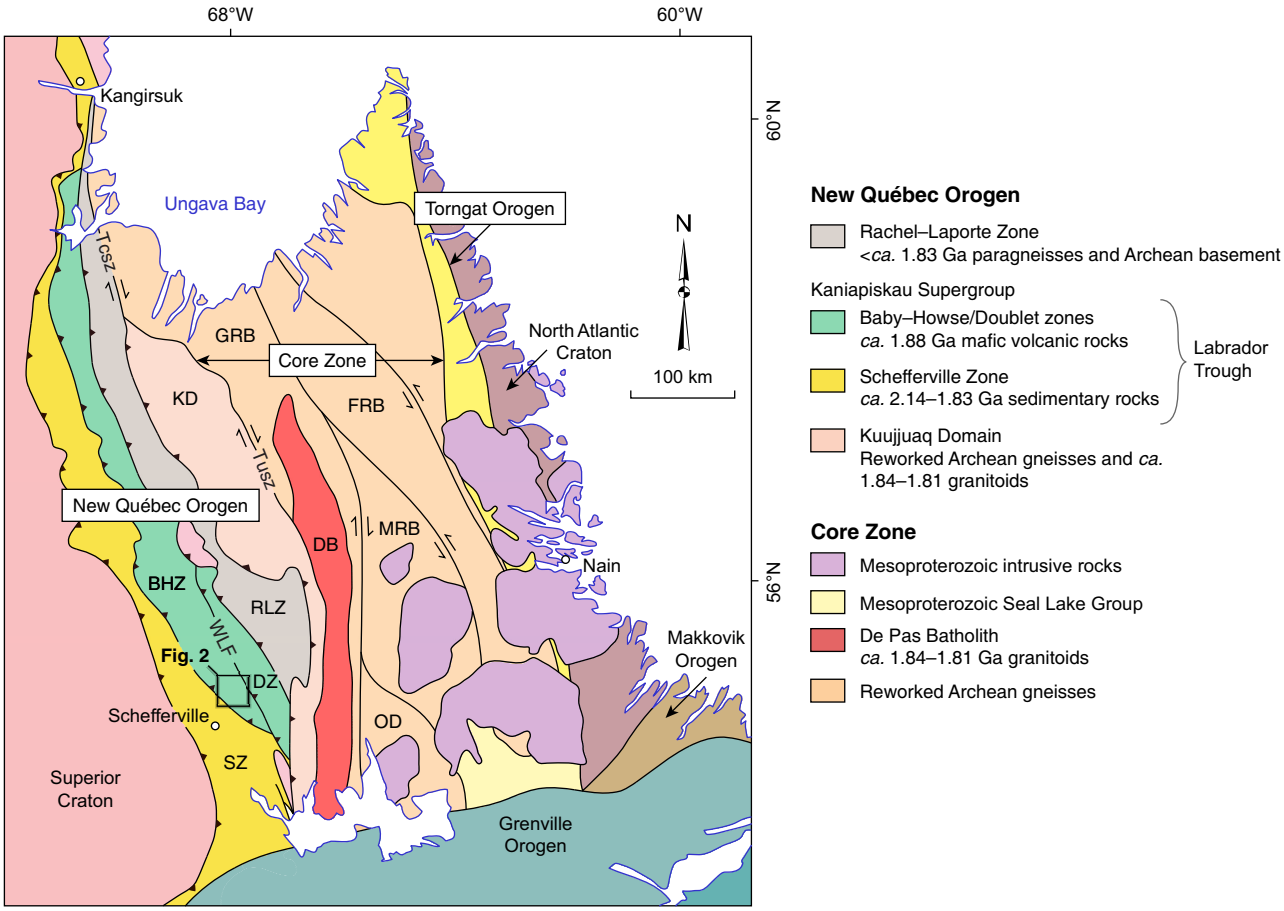

Figure 1. *Simplified geological map of northern Québec and Labrador emphasizing tectonic features discussed in the text (modified from Corrigan* et al.*, 2018). Abbreviations are as follows: SZ=Schefferville Zone; BHZ=Baby–Howse Zone; RLZ=Rachel–Laporte Zone; DZ=Doublet Zone; KD=Kuujjuaq Domain; DB=De Pas Batholith; GRB=George River Block; FRB=Falcoz River Block; MRB=Mistinibi-Raude Block; OD=Orma Domain; Tcsz=Lac Turcotte shear zone; Tusz=Lac Tudor Shear Zone; WLF=Walsh Lake Fault. "Fig. 2" box shows location of Hollinger Lake area (Figure 2).*

mafic–ultramafic sills (Findlay *et al.*, 1995); 3) an east-central domain (Rachel–Laporte Zone) underlain by amphibolite facies, *ca.* 1.83 Ga metasedimentary rocks of the Laporte Group (Henrique-Pinto *et al.*, 2017) and locally uplifted *ca.* 2.9–2.7 Ga basement (Machado *et al.*, 1989; Davis *et al.*, 2015; Rayner *et al.*, 2017); and, finally 4) an eastern domain (Kuujjuaq Domain; Perreault and Hynes, 1990) comprising amphibolite facies, late Archean to Paleoproterozoic gneisses, intruded by *ca.* 1.84–1.81 Ga granites (James and Dunning, 2000; Rayner *et al.*, 2017; Corrigan *et al.*, 2018). The Kuujjuaq Domain is bounded to the east by the dextral-transpressive Lac Tudor Shear Zone, east of which lies the Core Zone (CZ; James and Dunning, 2000; Corrigan *et al.*, 2009), an assemblage of Archean to Paleoproterozoic crustal blocks separated by a series of north–south-trending strike–slip shear zones. The westernmost of these domains, the George River Block (Corrigan *et al.*, 2019), is intruded by the De Pas Batholith, a large, north–south-trending granite suite comprising both deformed and undeformed plutons emplaced from *ca.* 1.84–1.81 Ga, and generally interpreted as a magmatic arc (Kerr *et al.*, 1994; Dunphy *et al.*, 1996).

Development of the NQO and southeastern THO is thought to have involved the closure of one or more ocean basins representing the present-day eastern extension of the Manikewan Ocean (Stauffer, 1984; Wardle *et al.*, 2002; Corrigan *et al.*, 2009, 2021), although the exact configuration of continental blocks and ocean basins remains unclear. Some tectonic interpretations (James and Dunning, 2000; Wardle *et al.*, 2002) have suggested multiple, east-dipping subduction zones to explain the presence of coeval (*ca.* 1.84 Ga) arc-related intrusions in the Kuujjuaq and George River domains, implying the former represents a micro-continent that was completely rifted from the Superior margin, and suggesting that a cryptic suture lies somewhere to the west, whereas others have invoked west-directed subduction or "double" subduction, *i.e.*, coeval west- and east-dipping

subduction along the Lac Tudor Shear Zone to explain these features (Corrigan *et al.*, 2018). Whatever the case, the available geochronological data indicate that crustal thickening began in the east, with high-temperature metamorphism of the Kuujjuaq Domain beginning by *ca.* 1836 Ma and persisting until *ca.* 1790–1780 Ma (*see* summary in Godet *et al.*, 2020), followed by somewhat later, *ca.* 1805–1780 Ma burial and metamorphism of the Rachel–Laporte Zone (Machado *et al.*, 1989; Godet *et al.*, 2020). The timing of deformation and metamorphism in the western (Schefferville, Baby–Howse and Doublet) zones is less constrained, owing to the low metamorphic grade and lack of datable units, but probably postdated *ca.* 1830 Ma, the youngest detrital zircon age obtained from deformed parts of the KS near Schefferville (D. Corrigan, personal communication, 2021), and had locally ceased by *ca.* 1813 Ma, the age of a post-tectonic monzonite intrusion cutting the deformed Cycle 2 Murdoch Formation (*see* below) near Nachicapau Lake, Québec (Machado *et al.*, 1997). Which of these ranges most closely corresponds to "terminal collision" in the NQO is not clear, and depends on which of the different tectonic reconstructions is adopted. For example, if the western NQO/KS and Rachel–Laporte Group/zone were originally separated by an ocean, as suggested by some reconstructions (*e.g.*, Henrique-Pinto *et al.*, 2017), then terminal collision may have been considerably later than 1830 Ma, but before *ca.* 1813 Ma.

REGIONAL STRATIGRAPHY OF THE KANIAPISKAU SUPERGROUP

The western part of the NQO, including the Martin Lake area (*see* below) is underlain by volcano–sedimentary rocks of the Kaniapiskau Supergroup (Figure 2; Clark and Wares, 2005). The KS is traditionally subdivided into three cycles (Wardle and Bailey, 1981; Clark and Wares, 2005): a lower, *ca.* 2.17 Ga rift–passive margin sequence (Cycle 1) comprising conglomerates and sandstones with minor associated alkaline basalts, turbidites and tholeiitic basalts, as well as shallow-water carbonates and siltstones; a second, *ca.* 1.88 Ga sequence (Cycle 2), represented to the west of the Walsh Lake Fault (Figures 1 and 3) by quartzite, iron formation, and turbidites of the Ferriman Group, and to the east by apparently coeval mafic volcanic and volcaniclastic rocks of the Doublet Group; and finally an upper, undated arkosic sandstone unit (Cycle 3) (the Tamarack River Formation in Labrador) generally interpreted as synorogenic molasse (Ware, 1980; Clark and Wares, 2005). Cycle 2 deposition in the south-central NQO was accompanied by local alkaline (*e.g.*, the Nimish Formation) volcanism as well as widespread intrusion of tholeiitic, *ca.* 1.88 Ga mafic to ultramafic sills (the Montagnais Sills; Skulski *et al.*, 1993; Findlay *et al.*, 1995; Conliffe *et al.*, 2019), the former with MORB-like geochemistry, and interpreted to indicate renewed, lithospheric-scale rifting along the eastern edge of the Superior Craton (Skulski *et al.*, 1993).

The Martin Lake area is primarily underlain by rocks corresponding to Cycle 2 of the KS, namely the Ferriman and Doublet groups. The age of the Ferriman Group, in the vicinity of the Martin Lake porphyry (Baby–Howse Zone), is constrained by a 1878.5 ± 0.8 Ma gabbro sill that intrudes the Menihek Formation slates near Howse Lake (Findlay *et al.*, 1995; Bleeker and Kamo, 2018), approximately 50 km along-strike of Martin Lake. The age of the Doublet Group in Labrador is less constrained; a single Pb–Pb age by Rohon *et al.* (1993) from the Willbob basalts of the Doublet Group yielded an imprecise age of 1885 ± 67 Ma, but it is generally considered to correlate with basalts and co-genetic *ca.* 1878 Ma gabbro sills of the Koksoak Group in the northern part of the orogen (Machado *et al.*, 1997; Clark and Wares, 2005).

GEOLOGY OF THE MARTIN LAKE AREA

Detailed maps of the Martin Lake area are available in industry reports by Auger (1949) and Bloomer (1954), and the area was included in regional geological surveys by Frarey (1967), Doherty (1979) and Butler (2018). The area is very poorly exposed, and field relations must be inferred from scattered outcrops combined with geophysical and topographic maps.

The Martin Lake porphyry crops out in the northeastern part of the Hollinger Lake map area (NTS 23J/16; Figure 2), where it forms a thin, approximately 1-km-thick lens extending from just north of Martin Lake, approximately 10 km east-southeastward. It is situated just south of the trace of the Walsh Lake Fault, which as noted above separates the Baby–Howse and Doublet tectonic zones, both of which are underlain by Cycle 2 volcano–sedimentary rocks of the KS (Wardle, 1982) and Montagnais gabbro sills. The Walsh Lake Fault is not exposed in the Hollinger Lake area, although it is apparent on regional aeromagnetic and topographic maps. Northeast of the trace of the fault, chlorite–phyllites and deformed pyroclastic rocks of the Murdoch Formation, overlying black shales (Thompson Lake Formation), and basalts (Willbob Formation) are deformed into a series of tight, west-verging folds. South of the trace of the fault, the area is underlain by a thick gabbro-sediment sill sequence overlain by greywackes and slates assigned to the Menihek Formation (Ferriman Group; Doherty, 1979; Wardle, 1982), all of which have been deformed into a broad, doubly plunging (northeast–southwest) syncline. A small, 0.5-km-thick by 3-km-long, fault-bounded lens comprising jasper-bearing conglomerates and sandstones of unclear stratigraphic affinity is sandwiched between the western end of the Martin Lake porphyry and

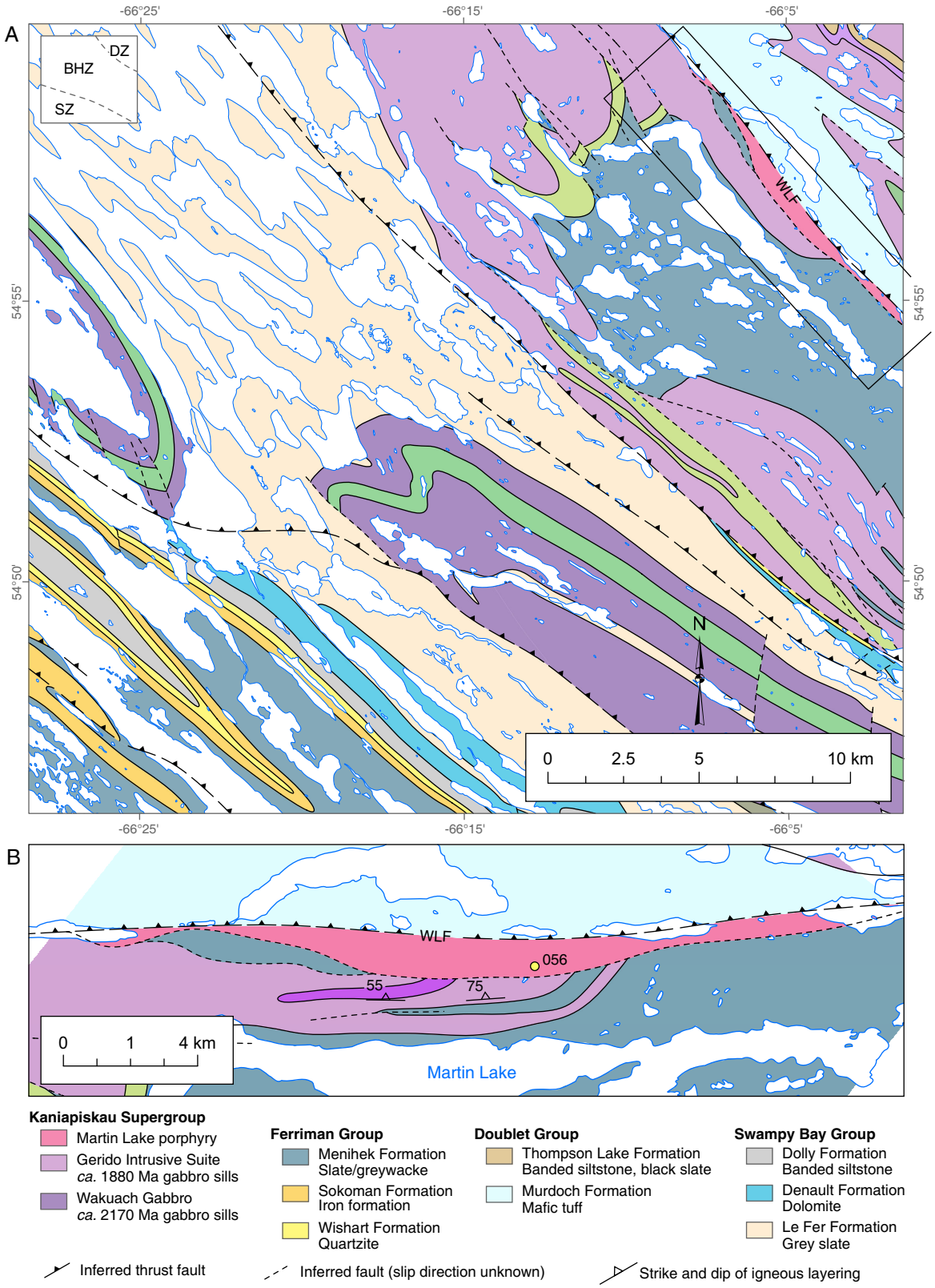

Figure 2. *A) Simplified geological map of the Hollinger Lake map area (NTS 23J/16). Square inset box in top left shows tectonic zones discussed in text. SZ=Schefferville Zone; BHZ=Baby–Howse Zone; DZ=Doublet Zone; WLF=Walsh Lake Fault; B) Geology of the Martin Lake area (rectangle in A) showing location of dated sample. Structural measurements from Wardle (1982).* See *Figure 3 and text for details of stratigraphy.*

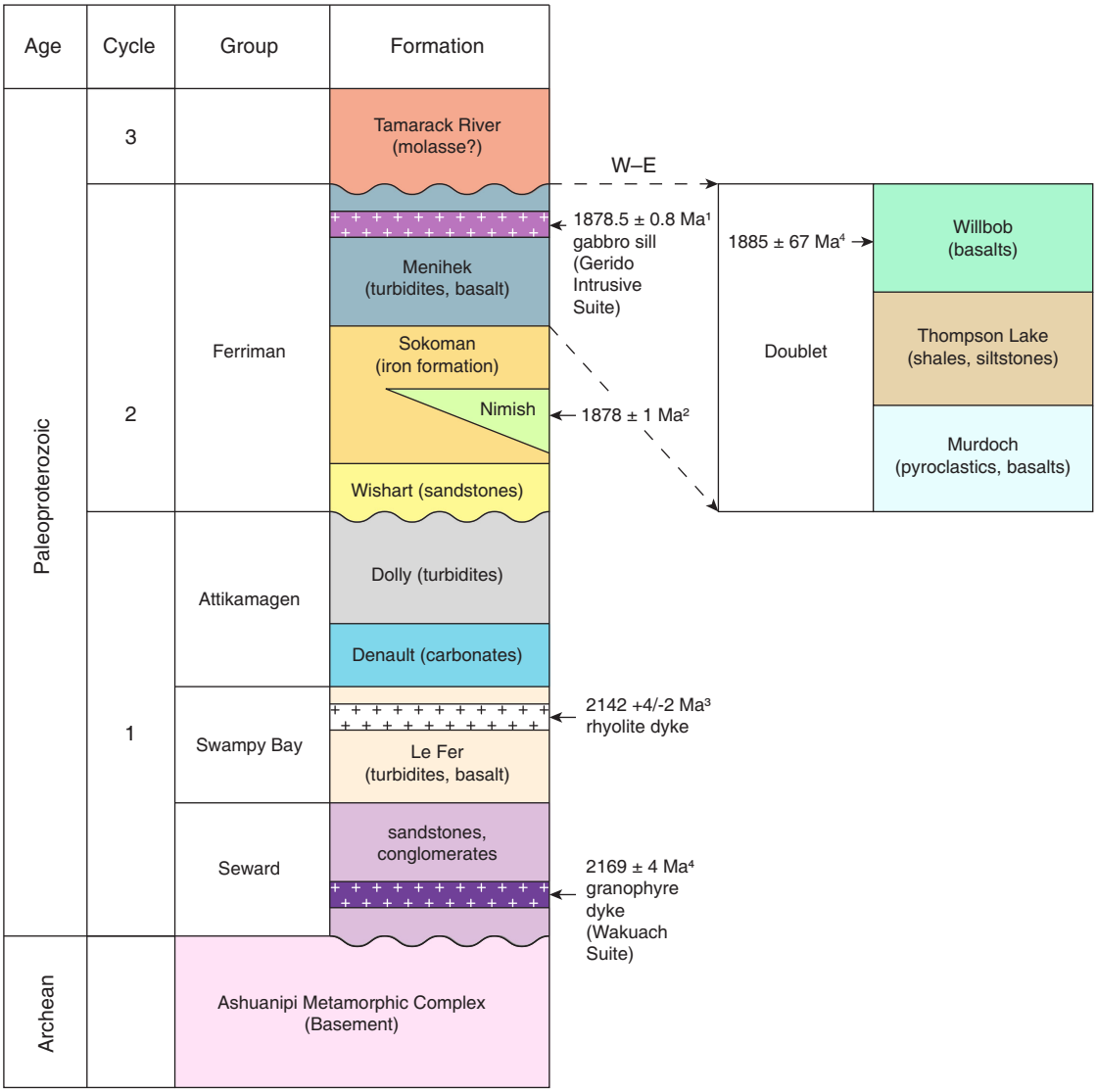

Figure 3. *Generalized stratigraphic column showing the main sedimentary units of the Kaniapiskau Supergroup in western Labrador (from Butler, 2020). The Doublet Group is considered to be correlative with the Cycle 2 Ferriman Group (*see *Clark and Wares, 2005). Geochronological data (with superscripts) from: 1) Bleeker and Kamo (2018); 2) Findlay* et al. *(1995); 3) T. Krogh and B. Dressler, cited by Clark (1984); 4) Rohon* et al. *(1993).*

the Walsh Lake Fault just north of the border in Québec (Auger, 1949). The latter were grouped by Wardle (1982) with the Menihek Formation, but they may alternatively correlate with basal conglomerates of the Murdoch Formation found locally to the northwest (Frarey, 1967; Wardle and Bailey, 1981), although neither have been examined in detail. The southern boundary of the Martin Lake porphyry, which is also not exposed, has been interpreted as a northeast-dipping thrust fault linked to the Walsh Lake Fault (Bloomer, 1954).

The metamorphic grade is low across most of the area, with gabbro sills south of the Walsh Lake Fault showing evidence of sub-greenschist-facies metamorphism (secondary chlorite, prehnite). The Murdoch Formation phyllites north of the fault are dominated by chlorite, with minor actinolite, suggesting greenschist-facies conditions. Deformation south of the Walsh Lake Fault is characterized by open to isoclinal folding, but aside from shearing along their margins the gabbros show little internal deformation, and the overlying Menihek Formation, whilst folded with an axial planar cleavage, is a low-grade slate. The Murdoch Formation, by comparison, exhibits a relatively strong, northeast-dipping foliation defined by a chlorite schistosity, local cm-scale planar quartz segregations, and the alignment of stretched volcanic clasts.

The Walsh Lake Fault has been interpreted as a northeast-dipping thrust fault having a strong dextral component (Frarey, 1967), or alternatively a west-dipping back-thrust (Dimroth, 1970). Wardle and Bailey (1981), in contrast, interpreted the fault as a syntectonic basin scarp associated with deposition of the Murdoch Formation, and suggested that rhyolite clasts, found within conglomerates at the base of the latter, indicated uplift and erosion of the Martin Lake porphyry during that time. The Menihek and Murdoch formations are locally conformable elsewhere in the orogen (Dimroth, 1970), suggesting only a minor offset. That said, the structure truncates regional-scale folds and so was clearly active during Hudsonian collision, although it is possible that it is a re-activated normal fault that experienced mostly dextral strike–slip motion.

The poor exposure of the Martin Lake porphyry makes it difficult to relate to the otherwise well-established regional stratigraphy. Auger (1949) interpreted the porphyry as intrusive, grouping it with gabbros in the Martin Lake area, noting that lithologically similar dykes were intruded into diorite and gabbro sills near the south end of nearby Vallant Lake. Bloomer (1954) later suggested rhyolite or a crystal tuff, with the latter implying a link to the volcaniclastic Murdoch Formation north of the Walsh Lake Fault. Frarey (1967) referred to the Martin Lake porphyry as "rhyolite", but, noting the lack of flow features, considered it intrusive, adding that it probably postdated nearby gabbro sills. The location of the Walsh Lake Fault immediately to the north of the unit suggests that it is at least partly fault bounded, and whereas its southern contact is less clearly defined, the linear distribution of outcrops suggests that it also cuts folded strata of the Ferriman Group.

The best exposures of the Martin Lake porphyry are located on the ridge just north of Martin Lake, although even these are limited to a few, several square-metre, mostly flat outcrops that provided little context. The unit there is massive, with sparse, mostly 0.5–1-cm-diameter, pink- to yellow-brown-weathered feldspar phenocrysts comprising up to 20% of the rock, in a dark-red/maroon aphanitic matrix (Plate 1A). No flow banding is apparent, and no other features indicative of an extrusive origin have been reported. Outcrops are complexly fractured and, in places, exhibit extensive brecciation (Bloomer, 1954). Seven samples were collected from the unit during regional mapping in 2017 and follow-up work in 2021, to clarify its age and origin. Observations and data from these are presented below.

PETROGRAPHY OF THE MARTIN LAKE PORPHYRY

Hand samples from the Martin Lake porphyry are divided into three textural types: dark-red porphyry having an aphanitic matrix (6 samples; Plate 1B), glassy red porphyry (1 sample; Plate 1C), and brecciated dark-red porphyry (1 sample; Plate 1D).

Petrographic descriptions of the Martin Lake porphyry are based on thin sections from the 3 samples collected during the 2017 field season, including one dark-red porphyry, one brecciated porphyry, and one glassy red porphyry. The samples have mostly retained their primary igneous textures, although most phenocrysts have been partly to completely replaced, and there is petrographic evidence that the unit has experienced considerable alteration. The dark-red porphyry sample contains phenocrysts of feldspar and a second unknown phase, which is now completely replaced by chlorite, set in a fine-grained matrix of quartz and K-feldspar, with titanomagnetite, rutile, apatite, and zircon present as accessory phases (Plate 2). Feldspar phenocrysts comprise about 15% of the rock, and are mostly fragments of rhombs or laths averaging about 1–5 mm in diameter (Plate 2A, B). Polysynthetic twinning is common, where not obscured by sericite alteration, and energy-dispersive X-ray spectroscopy (EDS) suggests that most of the phenocrysts are albite, although a few (not analyzed by EDS) exhibit microcline twinning. Most feldspar phenocrysts are isolated, but the glassy sample contains a few (5%) glomerocrysts comprising multiple plagioclase phenocrysts along with iron oxides and late hematite.

Small, typically 0.5-mm-diameter, equant, anhedral phenocrysts that probably represent an original Fe–Mg silicate (olivine or pyroxene?) replaced by chlorite comprise about 5% of the dark-red porphyry (Plate 2C). Magnetite forms irregular seams throughout these grains, interpreted as secondary replacement along fractures. Most grains contain several small inclusions of apatite and magnetite, the latter with oriented exsolution lamellae of rutile, and in places rutile appears to have largely overgrown the original magnetite.

The matrix consists of fine-grained intergrown quartz and K-feldspar that in plane-polarized light give the impression of a trachytic texture comprising weakly oriented quartz microlites with K-feldspar forming triangular to lath-shaped, interstitial grains (Plate 2A, E, F). Late chlorite is also present throughout the matrix, and may have replaced feldspar. The quartz microlites, many of which exhibit swallow-tail crystal terminations similar to plagioclase from quenched basalts (*e.g.*, Pearce, 1974), are part of larger, optically continuous quartz grains that have overgrown the original matrix texture. The matrix K-feldspar exhibits a distinct red colour, and cloudy appearance in thin section that appears to be related to fine-grained hematite inclusions. Large, round quartz grains surrounded by somewhat coarser grained (than the matrix) intergrown quartz, K-feldspar, and

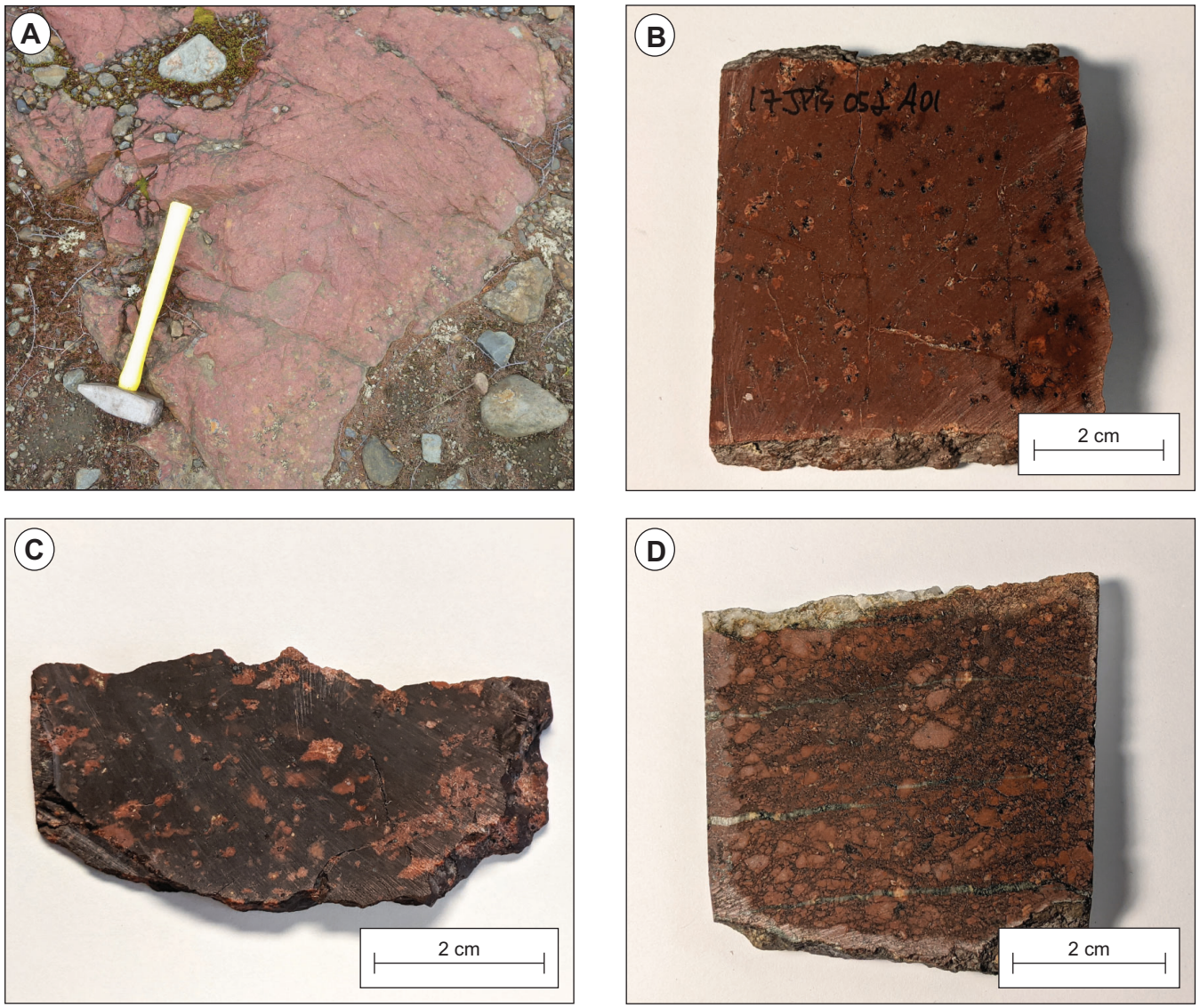

Plate 1. *A) Field photograph showing outcrop of the Martin Lake porphyry (hammer for scale); B–D) Cut slabs showing the dark-red porphyry (B), glassy red porphyry (C), and brecciated porphyry (D).*

late chlorite are dispersed throughout the matrix, and probably represent relict amygdules (Plate 2D).

The other samples are essentially textural variations on the dark-red porphyry. In the brecciated sample, angular fragments of dark-red porphyry (as described above) are separated by a network of black, oxide-filled (magnetite?) fractures, and cut by thin (0.5-mm-thick) quartz and chlorite veinlets, with the matrix adjacent to the veinlets appearing more intensely replaced by secondary quartz. The glassy red porphyry contains the same phenocryst assemblage (minus the inferred Fe–Mg silicate), but with more abundant feldspar glomerocrysts set in a cryptocrystalline quartzofeldspathic matrix.

ANALYTICAL METHODS AND RESULTS

WHOLE-ROCK LITHOGEOCHEMISTRY METHODS

Whole-rock major- and trace-element compositions were determined for 7 samples of the Martin Lake porphyry at the GSNL geochemical laboratory, following the analytical methods outlined by Finch *et al.* (2018). Major-element concentrations (in addition to Cr, Zr, Be, Sc and Ba) were analyzed by Inductively Coupled Plasma-Optical Emission Spectrometry (ICP-OES) following borate fusion. Ferrous iron (FeO) was calculated following the method of Wilson (1960). Volatiles were determined by loss-on-ignition at

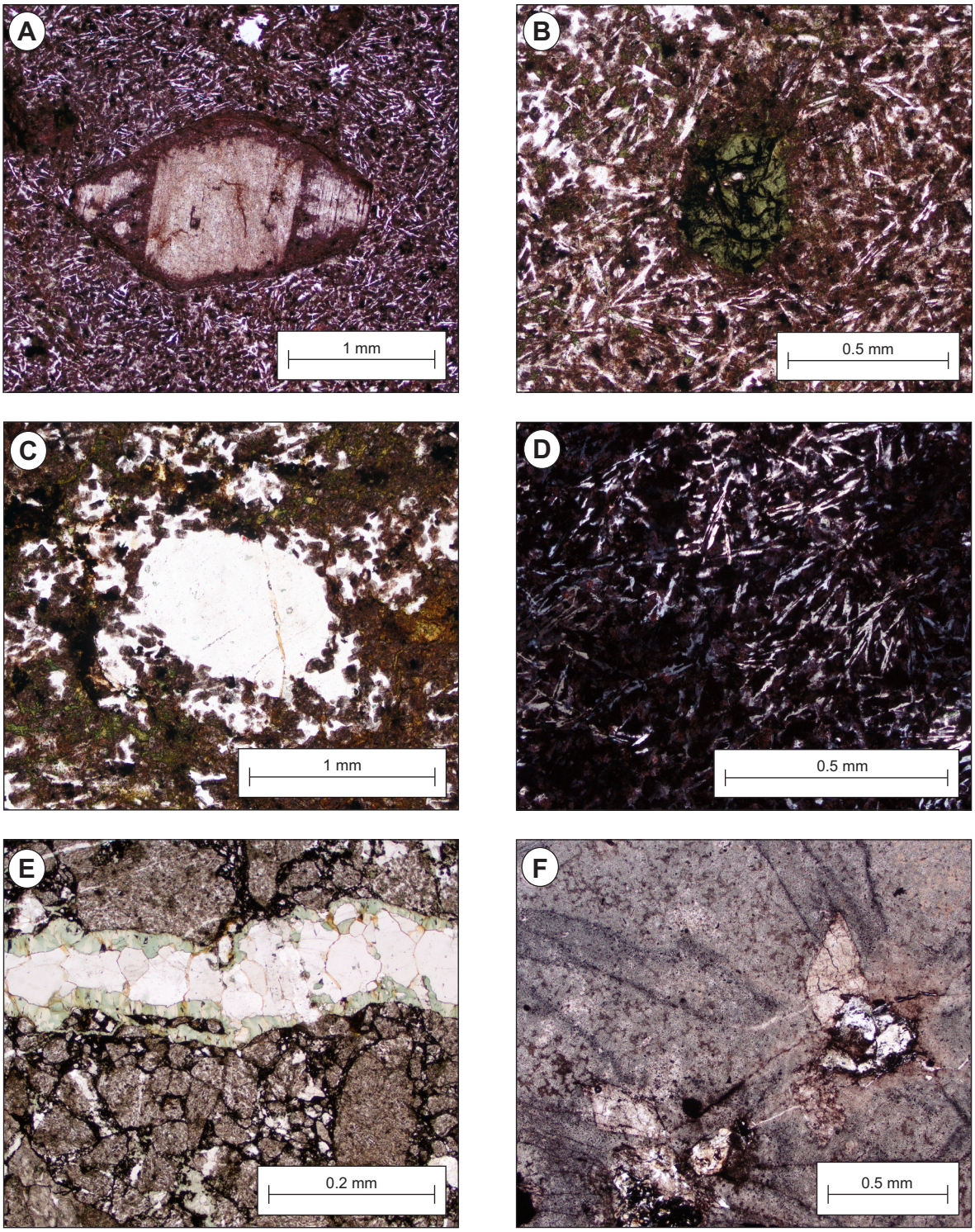

Plate 2. *Thin-section photographs showing the mineralogy and textures in the dark-red porphyry (A–D), brecciated porphyry (E) and glassy red porphyry (F). A) Strongly altered (sericitized) plagioclase phenocryst in quartz microlite and dusty K-feldspar matrix; B) Chlorite-altered inferred Fe–Mg phenocryst phase. Note extensive magnetite replacement along fractures; C) Ovoid quartz, probably an amygdule, surrounded by late chlorite; D) Close-up view (cross-polarized light) of matrix showing swallow-tail microlites overgrown by quartz; E) Brecciated porphyry with magnetite-filled fractures and late quartz + chlorite vein; F) Glassy red porphyry with feldspar phenocrysts in devitrified quartzofeldspathic matrix.*

1000°C. Rare-earth elements (REE) and selected trace elements were determined by Inductively Coupled Plasma-Mass Spectrometry (ICP-MS) following the same sample digestion procedure. Additional trace elements (As, Cd, Co, Cu, Li, Ni, Pb, Rb, V, Zn) were analyzed by ICP-MS following total acid digestion.

WHOLE-ROCK LITHOGEOCHEMISTRY RESULTS

Table 1 presents whole-rock major- and trace-element data for seven samples from the Martin Lake porphyry. The extent of major-element remobilization during post-emplacement alteration of the Martin Lake porphyry is difficult to assess with the small number of samples. On a Spitz and Darling (1978) plot (Figure 4A), the samples fall well within the "fresh to weakly altered" field, although there is some spread in Na_2O contents (2.27–4.31 wt. %). On the alteration box plot of Large *et al.* (2001; Figure 4B), two of the samples (one dark-red porphyry and the glassy porphyry) plot within the "least altered" (rhyolite) field, whereas the brecciated porphyry plots just outside the box along the chlorite–pyrite alteration vector, consistent with extensive secondary chlorite and magnetite. The four remaining dark-red porphyry samples, which have not been examined in thin section, plot to the right of the box, suggesting increased sericite alteration. Coupled with the aforementioned petrographic evidence for alteration, the concentrations of typically mobile elements in the Martin Lake porphyry samples should be treated with caution.

The major-element compositions of the Martin Lake porphyry are nonetheless consistent, and should be considered in the context of possible alteration types, although their use as indicators of primary magmatic affinity are probably limited. All samples are characterized by relatively high SiO_2 (66.58–73.14 wt. %), Na_2O (2.09–4.31 wt. %), K_2O (3.63–6.28 wt. %) and Al_2O_3 (11.31–12.46 wt. %), and low CaO (0.11–0.34 wt. %) and TiO_2 (~0.454–0.487 wt. %). Total iron in the non-brecciated samples ranges from 3.78–5.48 wt. %, with Mg varying from 0.11–0.78 wt. %. Higher total iron and Mg in the brecciated porphyry (7.44 and 2.72 wt. %, respectively) are consistent with more abundant magnetite and late chlorite in that sample. Loss-on-ignition (LOI) ranges from 0.63–1.49 wt. % in the non-brecciated samples, up to 2.10 wt. % in the brecciated sample.

Trace-element compositions of the Martin Lake porphyry samples are remarkably consistent, especially among the typically immobile elements. On the Nb/Y *vs.* Zr/TiO_2 diagram of Winchester and Floyd (1977), all samples are classified as rhyodacite/dacite (Figure 5A). All are enriched in high-field-strength elements (HFSE) (Zr=384–426 ppm; Y=39–51 ppm and Nb=17.5–21.7 ppm; Nb/Ta=14.0–16.9), and enriched in rare-earth elements (∑REE=410–467 ppm). With the exception of the brecciated sample, Large-Ion-Lithophile (LILE) concentrations are generally consistent, with notably high Ba=1034–1538 ppm and Rb=110–178 ppm, and relatively low Sr=50–86 ppm.

Primitive-mantle-normalized trace-element profiles (Figure 6A) are strongly fractionated ($(La/Yb)_{PM}$=11.16–14.99), with notable depletion in Nb (and Ta) relative to Th ($(Th/Nb)_{PM}$=9.49–11.70), in addition to P, and Ti, the latter consistent with fractionation of apatite and Fe-Ti oxides. Chondrite-normalized REE profiles (Figure 6B) are characterized by moderately inclined light rare-earth elements

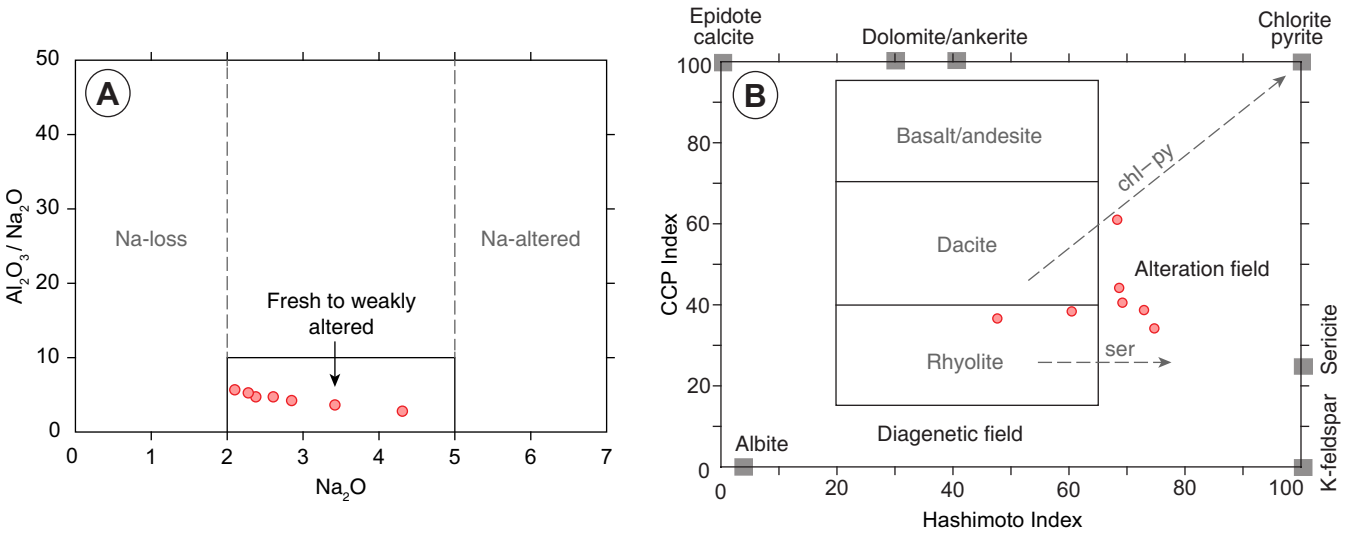

Figure 4. *A) Spitz and Darling (1978) plot for assessing the extent of alteration in the Martin Lake porphyry. Note that all samples plot within the "fresh to weakly altered" field, despite obvious alteration in thin section; B) Alteration box plot of Large* et al. *(2001).*

Table 1. Whole-rock lithogeochemical data for the Martin Lake porphyry. DRP=dark red porphyry; PGP=purple glassy porphyry; BP=brecciated porphyry

Sample	**17JPB052A01**	**17JPB054A01**	**17JPB208A01**	**21JPB0041A01**	**21JPB0042A02**	**21JPB0043A02**	**21JPB0044A02**
Lab Num	**11340022**	**11340023**	**11340097**	**11340185**	**11340186**	**11340187**	**11340188**
	DRP	**PGP**	**BP**	**DRP**	**DRP**	**DRP**	**DRP**
UTM_Zone	**19**	**19**	**19**	**19**	**19**	**19**	**19**
Easting	**685872**	**686733**	**690423**	**687501**	**687460**	**687345**	**687287**
Northing	**6093334**	**6092394**	**6088892**	**6091962**	**6091997**	**6092213**	**6092119**
Major elements (wt. %)							
SiO_2	69.97	71.61	66.58	71.31	73.14	72.07	69.62
TiO_2	.474	.481	.486	.466	.454	.47	.487
Al_2O_3	12.4	12.03	12.2	12.02	11.31	11.93	12.46
Fe_2O_{3tot}	4.45	4.67	7.43	4.76	5.62	3.78	5.48
Fe_2O_3	1.65	3.62	3.92	3.13	4.55	1.94	4.74
FeO	2.52	.94	3.16	1.47	.97	1.66	.67
MnO	.073	.016	.058	.045	.018	.032	.078
MgO	.78	.11	2.72	.51	.32	.56	.38
CaO	.34	.14	.11	.18	.13	.23	.27
Na_2O	3.42	4.31	2.85	2.27	2.37	2.09	2.6
K_2O	4.95	3.94	3.63	6.08	5.17	6.28	6.09
P_2O_5	.064	.063	.071	.065	.058	.063	.066
LOI	1.49	.63	2.1	1	1.1	.9	1.3
Total	98.42	98.	98.24	98.71	99.68	98.41	98.8
Trace elements (ppm)							
Cr	4	5	3	b.d.	b.d.	b.d.	b.d.
Ni	6	6	11	7	8	8	11
Sc	7.7	6.6	7.8	7.9	7.5	7.5	8
V	5	5	5	4	4	4	5
Cu	17	7	6	29	7	8	7
Pb	2	3	b.d.	5	3	10	8
Sn	3	4	4	4	2	3	3
Zn	59	23	103	43	36	54	32
Rb	146	110	89	172	146	158	178
Cs	.7	.8	b.d.	1	1.8	1.3	1.4
Ba	1186	1034	526	1465	1041	1440	1583
Sr	74	80	37	72	50	86	68
Ga	22	18	24	20	21	19	21
Ta	1.1	1.1	1.2	1.2	1.2	1.2	1.3
Nb	17.5	18.1	16.8	18.9	18.3	17.7	21.7
Hf	11.3	11	10.4	11.3	10.9	11.5	12.3
Zr	409	408	402	406	384	406	426
Y	42	39	44	44	39	45	51
Th	24.4	24.2	22.7	21.6	20.7	22.3	23.4
U	5.7	5	4.5	5.4	5.4	5.8	5.4
La	80.2	89.2	94	89.4	80.6	76.2	88.7
Ce	164.4	182.3	174.3	177.5	162.7	154	174.9
Pr	19	20.8	21.7	20	18.3	17.7	19.8
Nd	70.6	79.1	78	73	67.6	65.2	72.6
Sm	12	12.5	13	12.5	11.7	11.5	12.6
Eu	2.2	2.1	2.1	2.1	2	2.1	2.2
Gd	10.3	10.6	10.9	10.3	10	10	10.5
Tb	1.6	1.4	1.6	1.5	1.5	1.5	1.7
Dy	8.3	7.7	8.8	8.8	8.4	9	9.7
Ho	1.6	1.6	1.7	1.5	1.3	1.5	1.7
Er	5.1	5	5.2	4.9	4.3	5.1	5.5
Tm	.7	.7	.7	.6	.5	.6	.6
Yb	4.7	4.5	4.5	4.7	4.3	4.9	5.1
Lu	.7	.7	.7	.6	.5	.6	.6
ΣREE	429.5	462.2	467.2	457.8	418.9	410.8	463.6
Ratios							
Fe-number	76.36	89.52	53.74	74.24	75.19	74.77	63.81
Rb/Sr	1.97	1.38	2.41	2.39	2.92	1.84	2.62
Rb/Ba	.12	.11	.17	.12	.14	.11	.11
Th/U	4.28	4.84	5.04	4	3.83	3.84	4.33
Nb/Ta	15.91	16.45	14	15.75	15.25	14.75	16.69
Zr/Hf	36.19	37.09	38.65	35.93	35.23	35.3	34.63
Zr/Y	9.74	10.46	9.14	9.23	9.85	9.02	8.35
10 000×Ga/Al	3.35	2.83	3.72	3.14	3.51	3.01	3.18
$(La/Sm)_{PM}$	4.32	4.61	4.67	4.62	4.45	4.28	4.55
$(La/Yb)_{PM}$	12.25	14.22	14.99	13.65	13.45	11.16	12.48
$(Th/Nb)_{PM}$	11.7	11.22	11.33	9.59	9.49	10.57	9.05
$(La/Sm)_{CN}$	4.31	4.61	4.67	4.62	4.45	4.28	4.54
$(Gd/Yb)_{CN}$	1.81	1.95	2	1.81	1.92	1.69	1.7
Eu/Eu*	.61	.55	.53	.57	.56	.59	.59

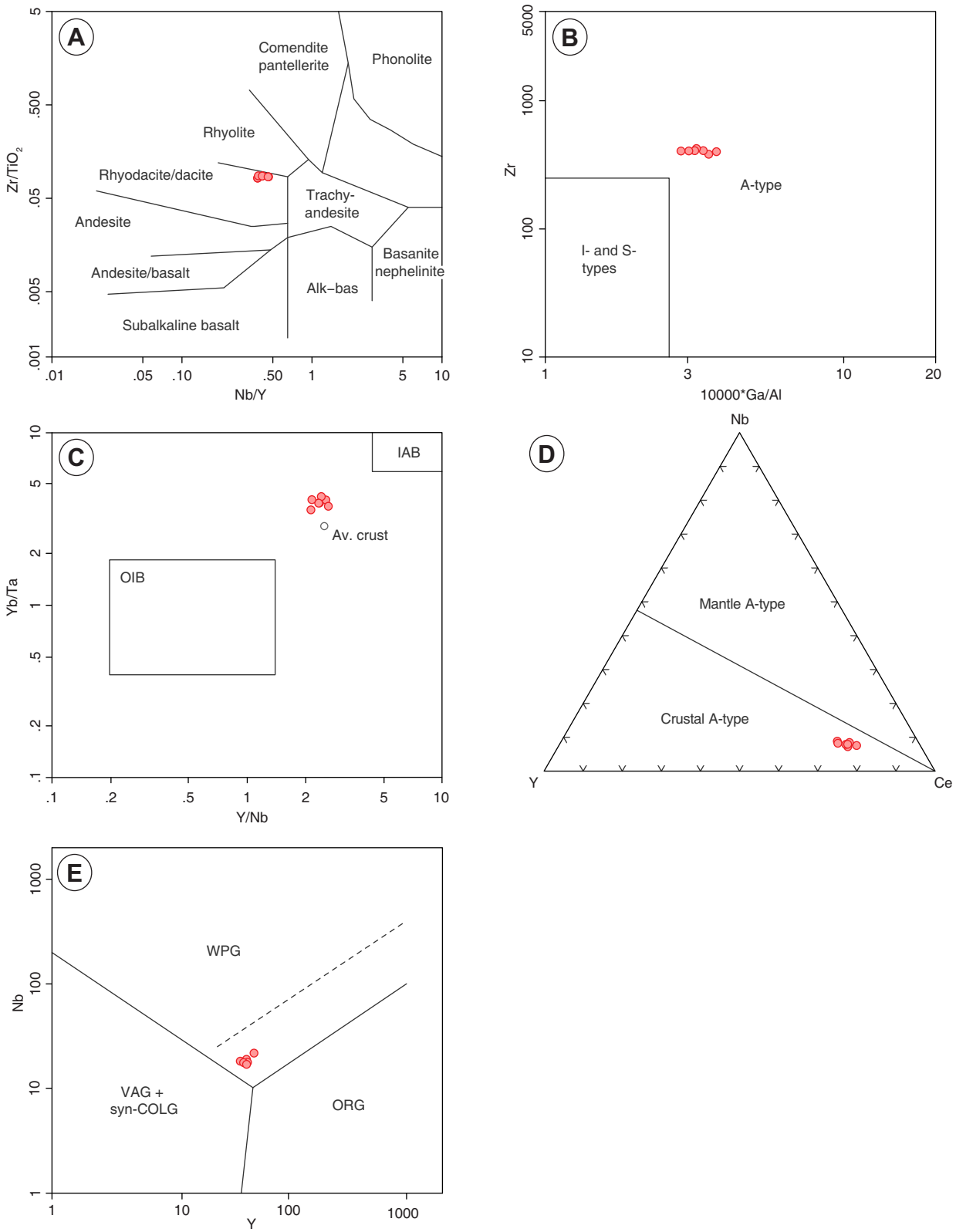

Figure 5. *Immobile-element-based classification diagrams for the Martin Lake porphyry. A) Nb/Y* vs. *Zr/TiO$_2$ classification diagram of Winchester and Floyd (1977); B) A-type granite classification diagram of Whalen* et al. *(1987); C) Y/Nb* vs. *Yb/Ta diagram of Eby (1990), showing similarity in composition of the Martin Lake porphyry to average crustal rocks; D) Mantle* vs. *crustal A-type granite diagram of Eby (1992); E) Granite classification of Pearce* et al. *(1984).*

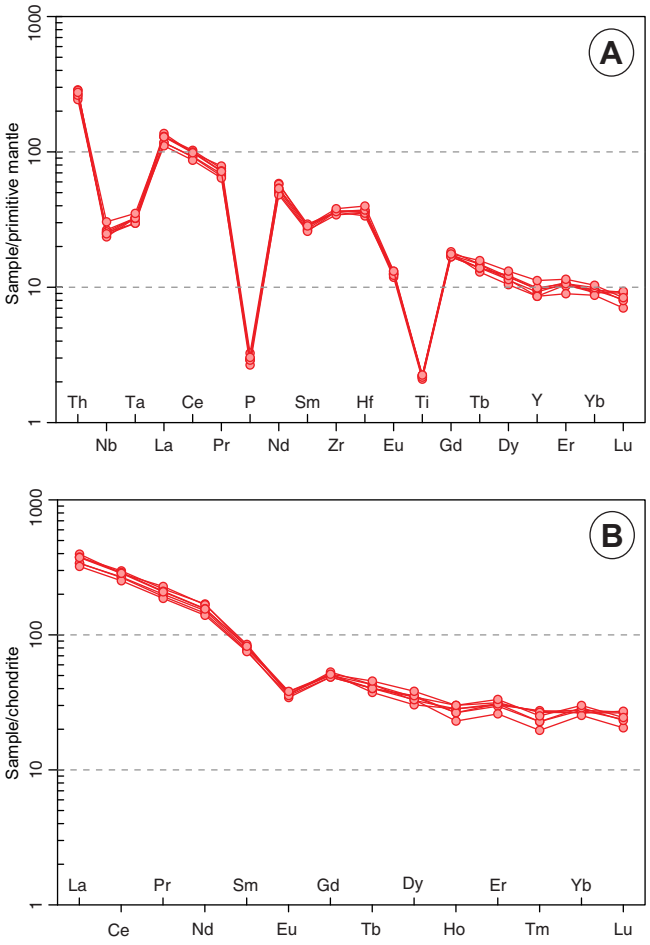

Figure 6. *A) Primitive-mantle-normalized trace-element profiles for the Martin Lake porphyry (normalization values from Sun and McDonough, 1989); B) Chondrite-normalized REE profiles for the Martin Lake porphyry (Sun and McDonough, 1989).*

(LREE; $(La/Sm)_{CN}$=4.31–4.67), relatively flat heavy-REE ($(Gd/Yb)_{CN}$=1.69–2.00), and negative Eu anomalies (Eu/Eu*=0.56–0.61), consistent with feldspar fractionation.

All samples contain relatively high Ga (19–24 ppm; 10 000×Ga/Al=2.83–3.72) for a given Zr content, similar to A-type granites (Whalen *et al.*, 1987; Figure 5B), and on the discrimination diagrams of Eby (1990, 1992), the samples plot within the fields of crustal or A2-type rocks. Finally, on the tectonomagmatic discrimination diagrams of Pearce *et al.* (1984), the samples plot in the "within-plate granite" field (Figure 5E).

U–Pb GEOCHRONOLOGY METHODS

Zircon U–Pb ages were determined by Chemical Abrasion-Isotope Dilution-Thermal Ionization Mass Spectrometry (CA-ID-TIMS) at the Jack Satterly Geochronology Laboratory, University of Toronto. The sample preparation, analytical and data processing methods follow those described by Hamilton and Buchan (2010) and Hamilton and Kerr (2016, and references therein). Extracted zircons were annealed at 900°C for 48 hours and then chemically abraded in HF for several hours following methods modified from Mattinson (2005). Isotopic ratios were measured using a single pulse-counting Daly detector on a solid source VG354 mass spectrometer.

Results of the U–Pb isotopic analysis are given in Table 2 and a concordia diagram (Figure 7). Analytical uncertainties are reported at the 2σ level.

U–Pb GEOCHRONOLOGY RESULTS

A sample of the Martin Lake porphyry yielded abundant good quality zircon and zircon fragments (Plate 3). The majority of grains are relatively clear and colourless to pale yellow-brown, and typically prismatic with square to slightly flat cross sections. Most contain small mineral and/or fluid inclusions; rare zircon grains are inclusion-free. Four of the highest-quality zircons were selected for analysis (fractions "Z1–Z4", Table 1; Plate 3, inset). The resulting data are mostly concordant, although fraction Z2 shows a minor amount of reverse discordance and has been excluded from further discussion and calculations. The other three analyses share a narrow range of $^{207}Pb/^{206}Pb$ ages from 1812.1–1814.7 Ma, and plot on concordia within the limits of the decay constant uncertainties (Figure 7). Free regression of these three fractions yields a concordia intercept age of 1811.2 ± 3.6 Ma (lower intercept *ca.* 700 Ma; 95% probability of fit). The Th/U contents of the analyzed grains range from 0.56–0.60, and, coupled with their morphology,

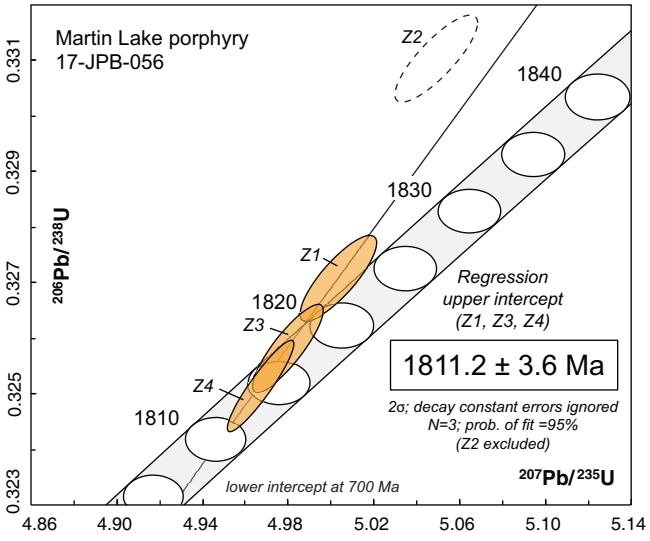

Figure 7. *U–Pb concordia diagram showing results of Martin Lake porphyry zircon analyses.* See *text for details.*

Table 2. Summary of U–Pb CA-ID-TIMS isotopic data for zircon from the Martin Lake porphyry

Analysis No.	Fraction	U (ppm)	Th/U	Pb_{tot} (pg)	Pb_c (pg)	$^{206}Pb/^{204}Pb$	$^{207}Pb/^{235}U$	2σ	$^{206}Pb/^{238}U$	2σ	Error Corr.	$^{207}Pb/^{206}Pb$	2σ	Age (Ma) $^{206}Pb/^{238}U$	2σ	Age (Ma) $^{207}Pb/^{235}U$	2σ	Age (Ma) $^{207}Pb/^{206}Pb$	2σ	% Disc.
MH19100	Z1; 1 clr, cls-pybr, brkn pr, incl	170	0.563	71.22	1.14	3679	5.00244	0.01443	0.327070	0.000624	0.8254	0.110928	0.000188	1824.2	3.0	1819.7	2.4	1814.7	3.1	-0.6
MH19101	Z2; 1 clr, cls-pybr, brkn el pr, incl	135	0.524	48.35	1.01	2851	5.04862	0.01576	0.331032	0.000665	0.7901	0.110612	0.000218	1843.4	3.2	1827.5	2.6	1809.5	3.6	-2.2
MH19102	Z3; 1 clr, cls shrp tip, incl	205	0.600	73.86	0.91	4746	4.97888	0.01327	0.325806	0.000643	0.8605	0.110834	0.000155	1818.0	3.1	1815.7	2.3	1813.1	2.5	-0.3
MH19130	Z4; 1 clr, cls, 2:1 flat pr, incl	105	0.578	38.35	0.22	10017	4.96590	0.01277	0.325132	0.000672	0.9219	0.110774	0.000116	1814.7	3.3	1813.5	2.2	1812.1	1.9	-0.2

Notes:
Z - zircon; all zircon grains have been thermally annealed and etched in conc. HF acid (Mattinson, 2005).
Abbreviations: clr - clear; cls - colourless; pybr - pale yellow-brown; brkn - broken; pr - prism/prismatic; shrp - sharp(ly faceted); incl - mineral or melt inclusion present.
Th/U calculated from radiogenic $^{208}Pb/^{206}Pb$ ratio and $^{207}Pb/^{206}Pb$ age, assuming concordance.
Pb_c is total common Pb, assuming the isotopic composition of laboratory blank ($^{206}Pb/^{204}Pb$=18.49 ± 0.4%; $^{207}Pb/^{204}Pb$=15.59 ± 0.4%; $^{208}Pb/^{204}Pb$=39.36 ± 0.4%).
$^{206}Pb/^{204}Pb$ corrected for fractionation and common Pb in the spike.
Pb/U ratios corrected for fractionation, common Pb in the spike, and blank.
Correction for ^{230}Th disequilibrium in $^{206}Pb/^{238}U$ and $^{207}Pb/^{206}Pb$ assuming a Th/U of 4.2 in the magma.
% Disc. is percent discordance for the given $^{207}Pb/^{206}Pb$ age.
Error Corr. is the correlation coefficient for X-Y errors in the Concordia plot.
Decay constants are those of Jaffey *et al.* (1971): ^{238}U = 1.55125 x 10^{-10}/yr, ^{235}U = 9.8485 x 10^{-10}/yr.

Plate 3. *Photographs showing a sample of best-quality zircons from the Martin Lake porphyry and (inset) analyzed grains Z1–Z4 (*see *Figure 7, Table 2 and text for details).*

suggest that the zircon is of primary igneous origin (Hoskin and Schaltegger, 2003).

Sm–Nd ISOTOPIC DATA

Sm–Nd isotopic compositions were determined for one sample of the Martin Lake porphyry at the Earth Resources Research and Analysis Facility at Memorial University, Newfoundland. The sample has a $^{143}Nd/^{144}Nd$ value of 0.511296, corresponding to $^{147}Sm/^{144}Nd$= 0.102200, a depleted mantle model age (T_{DM}) of 2399 Ma, and an initial $\varepsilon Nd_{(1811\ Ma)}$ value of -4.23. These results are discussed below.

Zr SATURATION TEMPERATURES

The temperature dependence of Zr solubility is commonly used to estimate magma temperatures in granitic rocks (Table 3; Hanchar and Watson, 2003). Calculated temperatures for the Martin Lake porphyry samples range from 876–899°C using the Zr saturation thermometry equations of Watson and Harrison (1983) and from 845–886°C using those of Boehnke *et al.* (2013). The results of these calculations are shown in Figure 8 along with contours of M (values from M=1.0–1.5 calculated following Watson and Harrison, 1983), which represents the compositional dependence of the thermometers (M=(Na+K+(2×Ca))/Al×Si)). The calculated temperatures should be interpreted with caution, because M depends on major-element ratios that in the Martin Lake porphyry have probably been modified by post-emplacement hydrothermal alteration (see discussion section). For example, if (as suggested by the textures) the unit has gained silica (which would lower M),

Table 3. Zr saturation temperature estimates for Martin Lake porphyry samples

Sample	Zr (ppm)	M	T_{Zr} (WH83)[a]	T_{Zr} (B13)[b]
17JPB052A01	409	1.38	876	848
17JPB054A01	408	1.39	874	845
17JPB208A01	402	1.10	899	886
21JPB0041A01	406	1.27	884	861
21JPB0042A02	384	1.21	884	864
21JPB0043A02	406	1.27	885	862
21JPB0044A02	426	1.34	883	857

Notes:
[a]Calculated following Watson and Harrison, 1983.
[b]Calculated following Boehnke *et al.*, 2013.

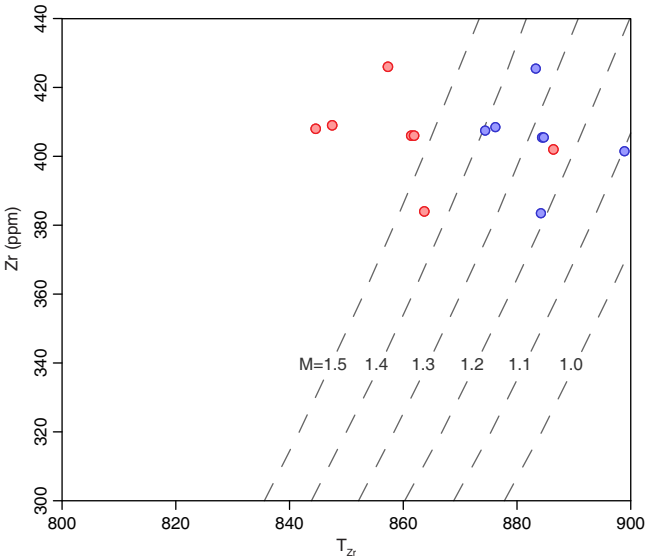

Figure 8. *Zr saturation temperatures (T_{Zr}* vs. *Zr (ppm)) calculated for the Martin Lake porphyry samples using the equations of Watson and Harrison (1983; blue dots) and Boehnke* et al. *(2013; red dots). Contours are M values (1.0–1.5) calculated using the equations of Watson and Harrison (1983).* See *text for details.*

then the calculated temperatures should be treated as maximum estimates. Nonetheless, the relatively high Zr contents of the porphyry (~400 ppm) are probably indicative of temperatures in excess of 800°C.

DISCUSSION

The origin of the Martin Lake porphyry has remained ambiguous since it was first mapped by Auger (1949), and many aspects, most notably its field relations, remain unclear. Petrographic features described above, including abundant broken phenocrysts, quench textures, and amygdules, together with its massive appearance in outcrop, suggest that the unit is a probably a subvolcanic intrusion. Other petrographic features hint at considerable post-emplacement alteration. The curious quartz microlite matrix texture of the porphyry can be explained by replacement of primary plagioclase microlites by quartz, as seen in some hydrothermally silica-altered andesites (Gibson *et al.*, 1983; Yamagishi and Dimroth, 1985), although none of the plagioclase phenocrysts in the porphyry have been silicified. Scanning electron microscopy imaging and EDS analyses show that the matrix of the porphyry consists almost entirely of these microlites intergrown with K-feldspar, suggesting that if they were originally plagioclase, then the rock is actually an altered trachyandesite/latite. The alternative is that the microlites represent primary quartz recrystallized during low-grade regional metamorphism. Primary quartz microlites are reported from some high-temperature rhyolites (Rowe *et al.*, 2012; Hanson and Eschberger, 2014), where they are interpreted as having originated as the high-temperature SiO_2 polymorph tridymite, but are rare. The presence of quartz + chlorite veins in some samples further supports a hydrothermal origin.

The geochemistry of the Martin Lake porphyry is reminiscent of A-type granites, a designation originally used to describe Fe-rich, low-H_2O granites derived from fractionation of alkaline basalts in anorogenic tectonic settings (Loiselle and Wones, 1979), but which has since been applied to almost any granite with "A-type geochemistry", namely high FeO/(FeO+MgO), K_2O/Na_2O, and HFSE (*e.g.*, Zr, Nb, Ta and Ga; Whalen *et al.*, 1987; Eby, 1990, 1992). It is now clear that A-type granites *s.l.* can originate from a variety of sources and tectonic environments, and consequently some authors have advocated replacing the term with the more general "ferroan", a non-genetic classification based on Fe-number (FeO/(FeO+MgO) >0.7–0.8) of which A-type granites are a subset (Frost *et al.*, 2001; Frost and Frost, 2011). The classification scheme for granites proposed by Frost *et al.* (2001) has not been applied here because the aforementioned alteration suggests that the major-element ratios of the Martin Lake porphyry are probably not representative of its primary magmatic composition, although all but two of the samples appear to be ferroan (Fe-number in Table 2). The porphyry has been classified here as A-type on the basis that it exhibits HFSE enrichment characteristic of A-type granites. The relatively high Zr saturation temperatures calculated for the porphyry samples (>800°C) are also typical of A-type granites (Turner *et al.*, 1992; King *et al.*, 1997; Wang et al., 2020).

A-type granites are typically thought to form from high-temperature, low-H_2O, halogen-rich melts (Eby, 1990).

Several different models have been proposed for their petrogenesis (*see* discussions in Eby, 1990; Whalen *et al.*, 1987; Martin, 2006; Frost and Frost, 2011; Janoušek *et al.*, 2020), ranging from fractionation from basaltic magmas with or without crustal contamination, to derivation by low-pressure partial melting of existing quartzofeldspathic crust. A detailed petrogenetic model for the Martin Lake porphyry is beyond the scope of this report, but the present data broadly support derivation by melting of pre-existing crust. The trace-element compositions of the porphyry are similar to the "A2-type" granites of Eby (1992), a subset of A-type granites characterized by relatively high Y/Nb, which is typical of average continental crust and generally thought to reflect derivation from lithosphere that has been depleted in Nb during arc magmatism. The Sm–Nd isotopic data also point to the involvement of an older crustal component in its petrogenesis. Figure 9 plots Age *vs.* $\varepsilon Nd_{(t)}$ for the porphyry together with unpublished data for nearby basalts and Archean granitoid rocks from the Andre Lake area (Table 4). Additional data for basalts and gabbros from a nearby part of the NQO are available from Rohon *et al.* (1993), but are not shown. The $\varepsilon Nd_{(1811\ Ma)}$ value of -4.23 for the Martin Lake porphyry lies within a range of values defined by the Paleoproterozoic mafic rocks having mildly depleted to slightly enriched $\varepsilon Nd_{(1811\ Ma)}$ values (+3.97 to -2.34), and Archean basement rocks with strong negative values (-11.48 to -13.25). The intermediate $\varepsilon Nd_{(1811\ Ma)}$ of the porphyry is too high to be explained by melting solely of Archean crust, implying the involvement of either a juvenile mantle-derived melt, or melting of a younger crustal component characterized by higher $\varepsilon Nd_{(t)}$. Given the absence of any coeval, *ca.* 1811 Ma mafic magmatism in the NQO, the most likely explanation is that the Martin Lake porphyry was derived from a crustal source comprising a mixture of Archean and Proterozoic components. The apparently very minor volume of crustal-sourced A-type/ferroan rocks of this age in the NQO is consistent with the observation of Frost and Frost (2013; citing Skjerlie and Johnston, 1993) that ferroan plutons formed by crustal melting are typically small because a large degree of melting will invariably produce melts that are magnesian and not ferroan.

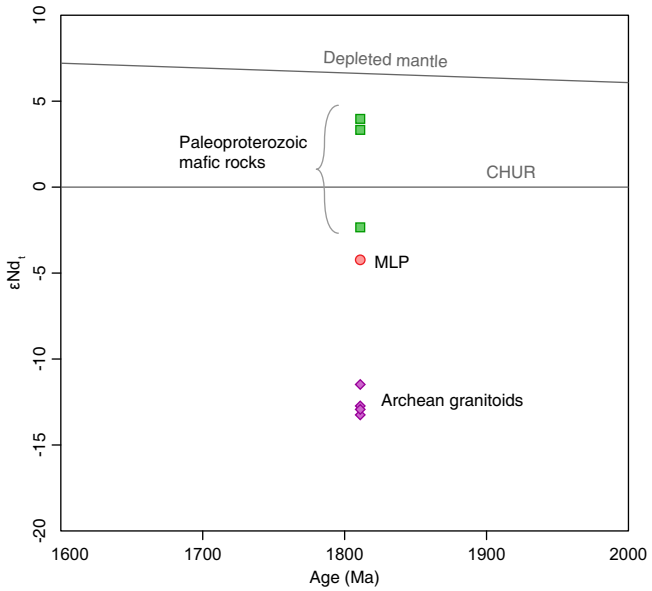

Figure 9. *Plot of Age (Ma)* vs. *εNd(t) for the Martin Lake porphyry and other Labrador Trough lithologies. εNd(t) are calculated for an age of 1811 Ma. Depleted mantle curve from DePaolo (1981).*

The *ca.* 1811 Ma age of emplacement for the Martin Lake porphyry overlaps with the *ca.* 1813 Ma age of an undeformed monzonite intruded into the Murdoch Formation near Nachicapau Lake, Québec (Dressler, 1981; Machado *et al.*, 1997), suggesting that A-type (and locally alkaline) magmatism, although of minor volume, occurred across a large part of the NQO at this time, and may be underreported, or simply not exposed. Emplacement of the Nachicapau Lake monzonite has been interpreted to date the cessation of deformation in the NQO because it cuts the

Table 4. Summary of Sm–Nd isotopic data for the Martin Lake porphyry and other Labrador Trough units

Sample	UTM Zone	Easting	Northing	Lithology	Nd (ppm)	Sm (ppm)	$^{147}Sm/^{144}Nd$ measured[a]	$^{143}Nd/^{144}Nd$	2σ	$\varepsilon Nd_{(t=1811\ Ma)}$[b]	T_{DM}[c]
18JPB046A01	20	331832	6060804	Willbob Fm. basalt	7.94	2.63	0.2000	0.512880	6	3.97	1769
17JPB054A01	19	686733	6092394	Martin Lake porphyry	74.88	12.66	0.1022	0.511296	12	-4.23	2399
18JPB017A01	20	308635	6049804	Nimish Fm. basalt	108.34	20.52	0.1145	0.511539	7	-2.34	2320
17JPB190A01	19	674850	6083509	Le Fer Fm. basalt	5.90	1.93	0.1983	0.512827	7	3.33	2125
18JPB170A01	20	317263	6051719	Snelgrove Lake granite	6.10	0.92	0.0910	0.510793	7	-11.48	2820
18JPB172A01	20	333314	6050275	MRD foliated granite	4.09	1.98	0.2934	0.513114	7	-13.25	-
18JPB173A01	20	335511	6053475	MRD biotite gneiss	37.36	4.79	0.0775	0.510558	7	-12.93	2804

Notes:
MRD=McKenzie River Domain
[a]Present study $^{143}Nd/^{144}Nd$ adjusted from the deviation to JNdi-1 Standard (accepted valve = 0.512115).
[b]Calculated using present day chrondritic uniform reservoir (CHUR) with $^{143}Nd/^{144}Nd$=0.512638 and $^{147}Sm/^{144}Nd$=0.1967.
[c]Calculated following DePaolo (1981).

dominant fabric in the Murdoch Formation (Machado *et al.*, 1997). Unfortunately, the field relations of the Martin Lake porphyry are somewhat ambiguous owing to its poor exposure. If the porphyry is pre-tectonic with respect to the Walsh Lake Fault, then deformation in the south-central NQO appears to have taken place later, or lasted somewhat longer than in the central part of the orogen, a reasonable interpretation given that deformation and high-grade metamorphism remained active in the hinterland across-strike from the Martin Lake area from *ca.* 1815–1802 Ma (James and Dunning, 2000).

The broader tectonic significance of *ca.* 1813–1811 Ma A-type magmatism in the NQO is not yet clear. A-type granites often form in extensional tectonic settings (Whalen *et al.*, 1987; Frost and Frost, 2011), including rifts and some back-arcs (Hinchey, 2021), but they are also typical components of "post-orogenic" magmatic suites (Turner *et al.*, 1992; Whalen *et al.*, 1996), where they are usually ascribed to high-temperature melting resulting from mantle upwelling owing to lithospheric delamination (*e.g.*, Kelly *et al.*, 2016), or tearing of the subducting slab (Whalen and Hildebrand, 2019). If the NQO was built by crustal accretion above an east-dipping subduction zone (*see* Regional Geology and Tectonics of the New Québec Orogen, this report), then emplacement of the Martin Lake porphyry must reflect some process within the subducting slab. Recent dating of prograde metamorphism of the Rachel–Laporte Zone implies that subduction was active until at least *ca.* 1805 (Godet *et al.*, 2020), and so large-scale lithospheric delamination or foundering at *ca.* 1813 Ma seems an unlikely explanation. Alternatively, if formation of the NQO was related to west-dipping subduction along the Lac Tudor Shear Zone, as suggested by Corrigan *et al.* (2018), then emplacement of the Martin Lake porphyry may have been related to upper-plate or back-arc extension. Further examination of similarly aged intrusions in the Kuujjuaq and George River domains may provide additional insight into the lithospheric structure of the orogen at this time.

CONCLUSIONS

The available field observations and petrographic data indicate that the Martin Lake porphyry is a lens-shaped subvolcanic unit, possibly a dyke, bounded by the Walsh Lake Fault to the north and a second subsidiary thrust to the south. It is generally massive in outcrop, and in thin section shows evidence of high-temperature, rapid emplacement followed by later, probably hydrothermal alteration that has largely obscured its primary mineralogy; it is either a rhyolite or alternatively a silica-altered trachyandesite/latite. The trace-element lithogeochemistry of the porphyry is similar to crustal-derived, A2-type granites, and together with relatively high Zr saturation temperatures (Table 3), implies high-temperature melting of a crustal source. The Sm–Nd isotopic data from the porphyry further support the involvement of older (Archean) lithosphere in its petrogenesis. The *ca.* 1811 Ma age of the porphyry overlaps with the age of alkaline intrusions in the central part of the NQO, pointing to similar, probably lithospheric-scale processes in their petrogenesis.

ACKNOWLEDGMENTS

Alana Hinchey, Hamish Sandeman, and John Hinchey provided thoughtful reviews of an early draft of this report. Sherri Strong (Memorial University) completed Sm–Nd analytical work. Dylan Goudie (Memorial University) completed sample preparation and provided support for SEM analytical work. Alana Hinchey, Benjamin MacDougall, Richard Bradbury and Richard Smith provided field assistance.

REFERENCES

Auger, P.E.
1949: Report on detailed geological mapping in the Frederickson-Faute-Martin Lake base metal zone. Newfoundland and Labrador Geological Survey, Assessment File LAB/0503, 24 pages.

Bleeker, W. and Kamo, S.L.
2018: Extent, origin, and deposit-scale controls of the 1883 Ma Circum-Superior large igneous province, northern Manitoba, Ontario, Québec, Nunavut and Labrador. *In* Targeted Geoscience Initiative: 2017 Report of Activities, Volume 2. *Edited by* N. Rogers. Geological Survey of Canada, Open File 8373, pages 5-14.

Bloomer, R.O.
1954: Report on the geology of the Martin Lake area, Labrador. Newfoundland and Labrador Geological Survey, Assessment File 23J/16/0071, 43 pages.

Boehnke, P., Watson, E.B., Trail, D., Harrison, T.M. and Schmitt, A.K.
2013: Zircon saturation re-revisited. Chemical Geology, Volume 351, pages 324-334.

Butler, J.P.
2018: New geological mapping of the Hollinger Lake area (NTS 23J/16), central Labrador Trough. *In* Current Research. Government of Newfoundland and Labrador, Department of Natural Resources, Geological Survey, Report 18-1, pages 193-206.

2020: Major- and trace-element geochemistry of mafic sills and dykes from the New Quebec Orogen, Western

Labrador. *In* Current Research. Government of Newfoundland and Labrador, Department of Natural Resouces, Geological Survey, Report, 20-1, pages 29-48.

Clark, T. and Wares, M.
2005: Lithotectonic and metallogenic synthesis of the New Québec Orogen (Labrador Trough). Ministère des Ressources Naturelles, Québec, MM 2005-01, 175 pages.

Conliffe, J., Smith, A. and Wilton, D.
2019: Petrographic, geochemical and sulphur isotope studies of gabbro sills, Labrador Trough: Implications for Ni–Cu–PGE exploration. *In* Current Research. Government of Newfoundland and Labrador, Department of Natural Resources, Geological Survey, Report 19-1, pages 1-21.

Corrigan, D., Rayner, N. and van Rooyen, D.
2019: Detrital zircon provenance and tectonostratigraphic evolution of the mid to southern Labrador Trough. GAC-MAC-IAH Québec 2019.

Corrigan, D. van Rooyen, D. and Wodicka, N.
2021: Indenter tectonics in the Canadian Shield: A case study for Paleoproterozoic lower crust exhumation, orocline development, and lateral extrusion. Precambrian Research, Volume 355, 106083.

Corrigan, D., Pehrsson, S., Wodicka, N. and De Kemp, E.
2009: The Palaeoproterozoic Trans-Hudson Orogen: a prototype of modern accretionary processes. Geological Society, London, Special Publications, Volume 327(1), pages 457-479.

Corrigan, D., Wodicka, N., McFarlane, C., Lafrance, I., van Rooyen, D., Bandyayera, D. and Bilodeau, C.
2018: Lithotectonic framework of the core zone, southeastern Churchill Province, Canada. Geoscience Canada, Volume 45(1).

Davis, D.W., Moukhsil, A., Lafrance, I., Hammouche, H., Goutier, J., Pilote, P. and Takam, T.F.
2015: Datations U-Pb dans les provinces du Supérieur, de Churchill et de Grenville effectuées au JSGL en 2012-2013, Volume RP 2014-07, pages 56.

DePaolo, D.J.
1981: A neodymium and strontium isotopic study of the Mesozoic calc-alkaline granitic batholiths of the Sierra Nevada and Peninsular Ranges, California. Journal of Geophysical Research: Solid Earth, Volume 86, pages 10470-10488.

Dimroth, E.
1970: Evolution of the Labrador geosyncline. Geological Society of America Bulletin, Volume 81(9), pages 2717-2742.

Doherty, R.A.
1979: Geological mapping in the Central Labrador Trough. *In* Report of activities for 1978. Government of Newfoundland and Labrador, Department of Mines and Energy, Mineral Development Division, Report 79-1, pages 129-134.

Dunphy, J.M., Skulski, T., Wardle, R.J. and Hall, J.
1996: Petrological zonation across the De Pas batholith: a tilted section through a continental arc. *In* Eastern Canadian Shield Onshore-Offshore (ECSOOT) Transect Meeting, pages 44-58.

Dressler, B.
1981: Post-tectonic igneous rocks: north-central Labrador geosyncline. Canadian Journal of Earth Sciences, Volume 18(11), pages 1758-1762.

Eby, G.N.
1992: Chemical subdivision of the A-type granitoids: petrogenetic and tectonic implications. Geology, Volume 20(7), pages 641-644.

1990: The A-type granitoids: a review of their occurrence and chemical characteristics and speculations on their petrogenesis. Lithos, Volume 26(1-2), pages 115-134.

Findlay, J.M., Parrish, R.R., Birkett, T.C. and Watanabe, D.H.
1995: U–Pb ages from the Nimish Formation and Montagnais glomeroporphyritic gabbro of the central New Québec Orogen, Canada. Canadian Journal of Earth Sciences, Volume 32, pages 1208-1220.

Finch, C., Roldan, R., Walsh, L., Kelly, J. and Amor, S.
2018: Analytical methods for chemical analysis of geological materials. Government of Newfoundland and Labrador, Department of Natural Resources, Geological Survey, Open File NFLD/3316, 67 pages.

Frarey, M.J.
1967: Willbob Lake and Thompson Lake map-areas, Quebec and Newfoundland (23 O/1 and 23 O/8). Geological Survey of Canada, Bulletin 348.

Frost, B.R., Barnes, C.G., Collins, W.J., Arculus, R.J., Ellis, D.J. and Frost, C.D.
2001: A geochemical classification for granitic rocks. Journal of Petrology, Volume 42(11), pages 2033-2048.

Frost, C.D. and Frost, B.R.
2011: On ferroan (A-type) granitoids: their compositional variability and modes of origin. Journal of Petrology, Volume 52(1), pages 39-53.

2013: Proterozoic ferroan feldspathic magmatism. Precambrian Research, Volume 228, pages 151-163.

Gibson, H.L., Watkinson, D.H. and Comba, C.D.A.
1983: Silicification; hydrothermal alteration in an Archean geothermal system within the Amulet Rhyolite Formation, Noranda, Quebec. Economic Geology, Volume 78(5), pages 954-971.

Godet, A., Guilmette, C., Labrousse, L., Smit, M.A., Davis, D.W., Raimondo, T., Vanier, M.A., Charette, B. and Lafrance, I.
2020: Contrasting PTt paths reveal a metamorphic discontinuity in the New Quebec Orogen: Insights into Paleoproterozoic orogenic processes. Precambrian Research, Volume 342, 105675.

Hall, J., Wardle, R.J., Gower, C.F., Kerr, A., Coflin, K., Keen, C.E. and Carroll, P.
1995: Proterozoic orogens of the northeastern Canadian Shield: new information from the Lithoprobe ECSOOT crustal reflection seismic survey. Canadian Journal of Earth Sciences, Volume 32(8), pages 1119-1131.

Hamilton, M.A. and Buchan, K.L.
2010: U–Pb geochronology of the Western Channel Diabase, northwestern Laurentia: Implications for a large 1.59 Ga magmatic province, Laurentia's APWP and paleocontinental reconstructions of Laurentia, Baltica and Gawler craton of southern Australia. Precambrian Research, Volume 183(3), pages 463-473.

Hamilton, M.A. and Kerr, A.
2016: New U–Pb dates from Silurian rocks on Fogo Island: Preliminary stratigraphic and tectonic implications. *In* Current Research. Government of Newfoundland and Labrador, Department of Natural Resources, Geological Survey, Report 16-1, pages 123-132.

Hanchar, J.M. and Watson, E.B.
2003: Zircon saturation thermometry. Reviews in Mineralogy and Geochemistry, Volume 53(1), pages 89-112.

Hanson, R.E. and Eschberger, A.M.
2014: An overview of the Carlton Rhyolite Group: Cambrian A-type felsic volcanism in the Southern Oklahoma Aulacogen. Oklahoma Geological Survey, Guidebook, Volume 38, pages 123-142.

Henrique-Pinto, R., Guilmette, C., Bilodeau, C. and McNicoll, V.
2017: Evidence for transition from a continental forearc to a collisional pro-foreland basin in the eastern Trans-Hudson Orogen: Detrital zircon provenance analysis in the Labrador Trough, Canada. Precambrian Research, Volume 296, pages 181-194.

Hinchey, A.M.
2021: Lithogeochemical and Nd isotopic constraints on felsic magmatism in the Makkovik Orogen, Labrador, Canada: Implications for assembly of the supercontinent Nuna. Lithos, Volume 382, 105917.

Hoskin, P.W. and Schaltegger, U.
2003: The composition of zircon and igneous and metamorphic petrogenesis. Reviews in Mineralogy and Geochemistry, Volume 53(1), pages 27-62.

James, D.T. and Dunning, G.R.
2000: U–Pb geochronological constraints for Paleoproterozoic evolution of the core zone, southeastern Churchill Province, northeastern Laurentia. Precambrian Research, Volume 103(1-2), pages 31-54.

Janoušek, V., Bonin, B., Collins, W.J., Farina, F. and Bowden, P.
2020: Post-Archean granitic rocks: contrasting petrogenetic processes and tectonic environments. Geological Society, London, Special Publications, Volume 491, pages 1-8.

Kerr, A., Fryer, B.J., Wardle, R.J., Ryan, B., Bridgwater, D. and Hall, J.
1994: Nd isotopic studies in the Labrador shield: progress report and preliminary data from the Torngat Orogen. *In* Eastern Canadian Shield Onshore–Offshore Transect (ECSOOT), Report of the 1993 Transect Meeting. The University of British Columbia, Lithoprobe Secretariat Report, Volume 36, pages 108-118.

Kelly, S., Butler, J.P. and Beaumont, C.
2016: Continental collision with a sandwiched accreted terrane: Insights into Himalayan–Tibetan lithospheric mantle tectonics? Earth and Planetary Science Letters, Volume 455, pages 176-195.

King, P.L., White, A.J.R., Chappell, B.W. and Allen, C.M.
1997: Characterization and origin of aluminous A-type granites from the Lachlan Fold Belt, southeastern Australia. Journal of Petrology, Volume 38(3), pages 371-391.

Konstantinovskaya, E., Ivanov, G., Feybesse, J.L. and Lescuyer, J.L.
2019: Structural features of the Central Labrador Trough: A model for strain partitioning, differential exhumation and late normal faulting in a thrust wedge under oblique shortening. Geoscience Canada, Volume 26, pages 5-30.

Large, R.R., Gemmell, J.B., Paulick, H. and Huston, D.L.
2001: The alteration box plot: A simple approach to understanding the relationship between alteration mineralogy and lithogeochemistry associated with volcanic-hosted massive sulfide deposits. Economic Geology, Volume 96(5), pages 957-971.

Loiselle, M.C. and Wones, D.R.
1979: Characteristics and origin of anorogenic granites. Geological Society of America, Annual Meeting Abstracts, Volume 11, page 468.

Machado, N., Goulet, N. and Gariépy, C.
1989: U–Pb geochronology of reactivated Archean basement and of Hudsonian metamorphism in the northern Labrador Trough. Canadian Journal of Earth Sciences, Volume 26(1), pages 1-15.

Machado, N., Clark, T., David, J. and Goulet, N.
1997: U–Pb ages for magmatism and deformation in the New Québec Orogen. Canadian Journal of Earth Sciences, Volume 34(5), pages 716-723.

Martin, R.F.
2006: A-type granites of crustal origin ultimately result from open-system fenitization-type reactions in an extensional environment. Lithos, Volume 91(1-4), pages 125-136.

Mattinson, J.M.
2005: Zircon U–Pb chemical abrasion ("CA-TIMS") method: combined annealing and multi-step partial dissolution analysis for improved precision and accuracy of zircon ages. Chemical Geology, Volume 220(1-2), pages 47-66.

Pearce, J.A., Harris, N.B. and Tindle, A.G.
1984: Trace element discrimination diagrams for the tectonic interpretation of granitic rocks. Journal of Petrology, Volume 25(4), pages 956-983.

Pearce, T.H.
1974: Quench plagioclase from some Archean basalts. Canadian Journal of Earth Sciences, Volume 11(5), pages 715-719.

Perreault, S. and Hynes, A.
1990: Tectonic evolution of the Kuujjuaq terrene, New Québec Orogen. Geoscience Canada. Volume 17(4), pages 238-240.

Rayner, N.M., Lafrance, I., Corrigan, D. and Charette, B.
2017: New U-Pb zircon ages of plutonic rocks from the Jeannin Lake area, Quebec: an evaluation of the Kuujjuaq domain and Rachel-Laporte Zone. *In* Current Research. Geological Survey of Canada, Report 2017-4. doi.org/10.4095/306180

Rowe, M.C., Ellis, B.S. and Lindeberg, A.
2012: Quantifying crystallization and devitrification of rhyolites by means of X-ray diffraction and electron microprobe analysis. American Mineralogist, Volume 97(10), pages 1685-1699.

Rohon, M.L., Vialette, Y., Clark, T., Roger, G., Ohnenstetter, D. and Vidal, P.
1993: Aphebian mafic–ultramafic magmatism in the Labrador Trough (New Quebec): its age and the nature of its mantle source. Canadian Journal of Earth Sciences, Volume 30(8), pages 1582-1593.

Skjerlie, K.P. and Johnston, A.D.
1993: Fluid-absent melting behavior of an F-rich tonalitic gneiss at mid-crustal pressures: implications for the generation of anorogenic granites. Journal of Petrology, Volume 34(4), pages 785-815.

Skulski, T., Wares, R.P. and Smith, A.D.
1993: Early Proterozoic (1.88–1.87 Ga) tholeiitic magmatism in the New Quebec orogen. Canadian Journal of Earth Sciences, Volume 30(7), pages 1505-1520.

Spitz, G. and Darling, R.
1978: Major and minor element lithogeochemical anomalies surrounding the Louvem copper deposit, Val d'Or, Quebec. Canadian Journal of Earth Sciences, Volume 15(7), pages 1161-1169.

Sun, S.S. and McDonough, W.F.
1989: Chemical and isotopic systematics of oceanic basalts: implications for mantle composition and processes. *In* Magmatism in the Ocean Basins. *Edited by* A.D. Saunders and M.J. Norry. Geological Society of London Special Publications, Volume 42, pages 313-345.

Stauffer, M.R.
1984: Manikewan: an early Proterozoic ocean in central Canada, its igneous history and orogenic closure. Precambrian Research, Volume 25(1-3), pages 257-281.

Turner, S., Sandiford, M. and Foden, J.
1992: Some geodynamic and compositional constraints on "postorogenic" magmatism. Geology, Volume 20(10), pages 931-934.

Wang, Y., Yang, Y.Z., Siebel, W., Zhang, H., Zhang, Y.S. and Chen, F.
2020: Geochemistry and tectonic significance of late Paleoproterozoic A-type granites along the southern margin of the North China Craton. Scientific Reports, Volume 10(1), pages 1-15.

Wardle, R.J.
1982: Geology of the south-central Labrador Trough. Government of Newfoundland and Labrador, Department of Mines and Energy, Mineral Development Division, Map 82-005.

Wardle, R.J. and Bailey, D.G.
1981: Early Proterozoic sequences in Labrador. *In* Proterozoic Basins in Canada. *Edited by* F.H.A. Campbell. Geological Survey of Canada, Paper 81-10, pages 331-358.

Wardle, R.J., James, D.T., Scott, D.J. and Hall, J.
2002: The southeastern Churchill Province: Synthesis of a Paleoproterozoic transpressional orogen. Canadian Journal of Earth Sciences, Volume 39, pages 639-663.

Ware, M.J.
1980: Tamarack River Formation, Sims Lake–Menihek Lake area, western Labrador. *In* Current Research. Government of Newfoundland and Labrador, Department of Mines and Energy, Mineral Development Division, Report 80-1, pages 194-200.

Watson, E.B. and Harrison, T.M.
1983: Zircon saturation revisited: temperature and composition effects in a variety of crustal magma types. Earth and Planetary Science Letters, Volume 64(2), pages 295-304.

Whalen, J.B., Jenner, G.A., Longstafffe, F.J., Robert, F. and Gariépy, C.
1996: Geochemical and isotopic (O, Nd, Pb and Sr) constraints on A-type granite petrogenesis based on the Topsails igneous suite, Newfoundland Appalachians. Journal of Petrology, Volume 37, pages 1463-1489.

Whalen, J.B., Currie, K.L. and Chappell, B.W.
1987: A-type granites: geochemical characteristics, discrimination and petrogenesis. Contributions to Mineralogy and Petrology, Volume 95(4), pages 407-419.

Whalen, J.B. and Hildebrand, R.S.
2019: Trace element discrimination of arc, slab failure, and A-type granitic rocks. Lithos, Volume 348, 105179.

Wilson, A.D.
1960: The micro-determination of ferrous iron in silicate minerals by a volumetric and a colorimetric method. Analyst, Volume 85(1016), pages 823-827.

Winchester, J.A. and Floyd, P.A.
1977: Geochemical discrimination of different magma series and their differentiation products using immobile elements. Chemical Geology, Volume 20, pages 325-343.

Yamagishi, H. and Dimroth, E.
1985: A comparison of Miocene and Archean rhyolite hyaloclastites: evidence for a hot and fluid rhyolite lava. Journal of Volcanology and Geothermal Research, Volume 23(3-4), pages 337-355.